Research Square

Preprints are preliminary reports that have not undergone peer review.
They should not be considered conclusive, used to inform clinical practice,
or referenced by the media as validated information.

Oscillating-plate ultrasonication of wheat gluten-water-extractable arabinoxylan composites: Structural reorganization and in vitro digestibility

Menglong Liu
Henan University of Science and Technology
Shaokai Wang
Henan University of Science and Technology
Hongyan Li
Henan University of Science and Technology
Yuanyuan Chen
Henan University of Science and Technology
Chonghui Yue
Henan University of Science and Technology
Peiyan Li
Henan University of Science and Technology
Denglin Luo
Henan University of Science and Technology
Jinying Guo
Henan University of Science and Technology
Zhouya Bai
spbaizhouya@163.com
Henan University of Science and Technology

Research Article

Keywords: water-extracted arabinoxylan, oscillating-plate ultrasound, gluten proteins, protein–polysaccharide interactions, in vitro digestion, wastewater valorization

Posted Date: November 4th, 2026

DOI: https://doi.org/10.21203/rs.3.rs-11364706/v1

License: This work is licensed under a Creative Commons Attribution 4.0 International License.
Read Full License

Additional Declarations: No competing interests reported.

Oscillating-plate ultrasonication of wheat gluten-water-extractable arabinoxylan composites: Structural reorganization and in vitro digestibility

Menglong Liu[a], ShaoKai Wang, Hongyan Li[a], Yuanyuan Chen[a], Chonghui Yue[a], Peiyan Li[a], Denglin Luo[ab], Jinying Guo[a*], Zhouya Bai[ab]*

a College of Food and Bioengineering, Henan University of Science and Technology, 471023, Luoyang, Henan, PR China

b Henan Food Raw Material Engineering Technology Research Center (Henan University of Science and Technology), Luoyang, 471023, China

* Corresponding author:

Zhouya Bai;

Tel& Fax: +86-13177788278;

E-mail address: spbaizhouya@163.com

Jinying Guo;

Tel& Fax: +86-13403790464;

E-mail address: guojinying8@163.com

Abstract：

This study investigated the effects of oscillating-plate ultrasonication on wheat gluten composites containing water-extractable arabinoxylan (WEAX) recovered from wheat gluten processing wastewater. Composites were treated at 40 kHz and a nominal power of 600 W for 0–40 s and characterized by textural, rheological, microscopic, spectroscopic, and in vitro gastrointestinal digestion analyses. WEAX incorporation altered gluten network organization and secondary-structure distribution, reducing hardness by 15.05% and gastric apparent digestibility by 34.31%, while increasing springiness by 14.67%. Ultrasonication induced duration-dependent structural changes, with hardness reaching its highest numerical value of 197.77 ± 18.08 g at 20 s. Changes in disulfide content were accompanied by redistribution of hydrophobic, hydrogen-bonding, and ionic interaction-related fractions. WEAX redistribution and gluten conformational rearrangement may have contributed to these responses. Ultrasonication partly alleviated the WEAX-associated reduction in gastric apparent digestibility, which reached 32.48 ± 0.60% at 30 s but remained below that of gluten without WEAX. Intestinal apparent digestibility showed a numerical decrease followed by recovery with longer treatment. The different treatment durations yielding the highest numerical hardness and gastric apparent digestibility indicate distinct responses of texture and digestive behavior. These findings provide a basis for selecting ultrasonication conditions according to the desired properties of WEAX–gluten composites and for further evaluation of wastewater-recovered WEAX as a cereal protein modifier.

Keywords: water-extracted arabinoxylan; oscillating-plate ultrasound; gluten proteins; protein–polysaccharide interactions; in vitro digestion; wastewater valorization

1. Introduction

Wheat is one of the most widely produced and consumed cereal crops in the world. Its industrial processing generates large quantities of gluten protein by-products (Mika & Wikiera, 2024). However, natural gluten proteins form a highly dense three-dimensional network via disulfide bonds, hydrogen bonds and hydrophobic interactions. The peptide chains are tightly folded and the enzyme cleavage sites are deeply embedded. This results in both inherent functional deficiencies and low digestibility and bioavailability in the body, making it difficult to meet the requirements for high-end nutritional foods and specialised dietary products (M. Zhang et al., 2023). Consequently, improving the digestibility of proteins by regulating their multiscale structures through green, efficient, and targeted modification technologies has become a core research focus in the field of grain protein processing.

Non-starch polysaccharides offer residue-free processing and align with the clean-label trend (Q. Guo et al., 2024). Gluten flour production also generates concentrated organic wastewater containing active polysaccharides such as arabinoxylans. Its direct discharge causes environmental burdens and wastes potentially valuable resources (Bai et al., 2024). Recovering arabinoxylan from this wastewater and using it as a protein modifier could therefore promote high-value utilization of wheat-processing by-products and support low-carbon food processing (Wan et al., 2025a). Arabinoxylan consists mainly of β-D-xylopyranose units linked by β-1,4 glycosidic bonds, with arabinose side chains and abundant hydroxyl groups

that can interact with gluten proteins through hydrogen bonding, hydrophobic interactions, and electrostatic forces (W. Liu et al., 2026). Moderate water-extractable arabinoxylan (WEAX) can penetrate the gluten network, compete for water, and create steric hindrance, thereby weakening direct protein association and loosening protein aggregates (Wan et al., 2025b). However, WEAX may also form a physical barrier that limits pepsin–protein contact during gastric digestion, while its mainly noncovalent interactions may not sufficiently disrupt the compact protein conformation (J. Hong et al., 2024).

Ultrasonic treatment is a typical non-thermal physical processing technology characterised by its high efficiency and environmental friendliness. It causes less thermal damage to proteins and offers greater processing efficiency, providing significant benefits for the modification of plant proteins and the development of composite systems (T. Wang et al., 2026). Existing research has demonstrated that ultrasound can effectively modulate the interfacial interactions between polysaccharides, such as inulin, and gluten proteins. Ultrasound promotes enhanced hydrophobic interactions, disulfide bond restructuring and ordering of secondary structures. This synergistically optimises the viscoelasticity, thermal stability and microstructure of the gluten network. Moreover, these modulatory effects are closely related to the molecular chain length and degree of polymerisation of the polysaccharides (Bai et al., 2026a). Our team has independently developed a vibrating-plate ultrasonic processing device and conducted preliminary research into its impact on the quality of dough processing and gluten protein structure (X. Li et al.,

2024; Meng et al., 2026). However, current research has largely focused on improving the quality of processing and the structural characteristics. There is still a lack of systematic, in-depth studies on how gluten proteins evolve dynamically and the underlying mechanisms of their gastrointestinal digestibility following ultrasonic-polysaccharide synergistic treatment.

This study examined gluten composites containing 2% (w/w) wastewater-recovered WEAX subjected to oscillating-plate ultrasound for 0-40 s, using gluten without WEAX as a reference. Texture, dynamic rheology, scanning electron microscopy (SEM), sulfhydryl/disulfide measurements, FTIR, Raman and circular dichroism (CD) spectroscopy, andl in vitro digestion were combined to characterize treatment-dependent responses. The objective was to examine how composite structural organization was associated with processing functionality and digestive behavior, providing a basis for further evaluation of recovered WEAX as a cereal protein modifier.

2. Materials and methods

2.1 Materials

The gluten protein is sourced from Henan Feitian Biotechnology Co., Ltd. (Hebi, China). The ultrasonic equipment uses a proprietary vibrating-plate ultrasonic system manufactured by Farang Ultrasonic Technology Co., Ltd. (based in Hangzhou, China), operating at a frequency of 40 kHz with a continuously adjustable power range of 0-720 W. The effective working surface area is 288 mm × 188 mm. Twelve built-in 60 W transducers are evenly distributed across the surface to ensure uniform

ultrasonic treatment.

2.2 Extraction of WEAX

Wheat gluten processing wastewater was centrifuged at 4000 rpm for 15 min. The supernatant was concentrated to one quarter of its original volume by rotary evaporation, mixed with four volumes of 95% ethanol, and left overnight. The precipitate obtained after centrifugation at 4000 rpm for 15 min was redispersed in water, dialyzed for 24 h, and freeze-dried to obtain crude WEAX.

Pretreated DEAE-52 cellulose was added to a 10 mg/mL solution of crude arabinoxylan, and the mixture was shaken at 120 rpm and 25°C for 6 h in a sealed flask. After centrifugation at 5000 rpm for 10 min, the polysaccharide-containing supernatant was precipitated with four volumes of 95% ethanol for 12 h. The precipitate was redissolved in water, concentrated by rotary evaporation, and freeze-dried (Wan et al., 2025).

The composition, molecular characteristics, and physicochemical properties of wastewater-derived WEAX were characterized in our previous study (Geng et al., 2024). The purified WEAX contained 92.99 ± 3.26% total sugars and 6.74 ± 1.39% residual protein, indicating improved purity compared with the crude extract, which contained 57.11% total sugars and 12.91% protein. WEAX comprised a xylose backbone with arabinose substituents. On a dry basis, xylose and arabinose accounted for 43.77% and 38.08%, respectively, yielding an arabinose-to-xylose (A/X) ratio of 0.87 and indicating a high degree of substitution. Galactose (10.51%) and glucose (5.86%) were also detected. The average molecular weight was 4.57×10^4 Da, with a

bimodal distribution. WEAX exhibited favourable thermal stability, shear-thinning behaviour, and weak gel characteristics. Its abundant hydroxyl groups may facilitate hydrogen bonding with gluten proteins, thereby contributing to changes in the microstructure and mechanical properties of dough systems.

2.3 Preparation of samples

(1) Control group: Accurately weigh out 10 g of gluten flour and place it in a beaker. Add 20 mL of deionised water and stir until uniform (M. Liu et al., 2021a).

(2) AX-0s group: Samples were prepared using the formulation described in (1), with WEAX added at 2% (w/w, based on the mass of gluten flour). WEAX was dispersed in distilled water, followed by the addition of gluten flour. The mixture was stirred until the gluten flour had fully absorbed the water and WEAX was uniformly distributed.

(3) Ultrasonic group: Follow the remaining steps as in (2). Once the pre-reaction is complete, transfer the sample to the sample chamber of the ultrasonicator. Set the ultrasonic power to 600 W and the frequency to 40 kHz. Then, perform ultrasonic treatment for the duration specified in the experimental requirements (10-40 s).

2.4 Determination of Texture Properties

Weigh 3 g of the prepared sample. The textural properties of these samples were then measured using a texture analyzer (Stable Micro Systems Co., Ltd., Surrey, UK) fitted with a P/75 probe. The test was performed under the following conditions: pre-test speed of 1.0 mm/s, test speed of 1.0 mm/s, post-test speed of 1.0 mm/s, 60% compression, a 5 s interval, and a trigger force of 5 g (Bai et al., 2026b).

2.5 Determination of Dynamic Rheological Properties

Strain and frequency sweeps were performed using a DHR-3 rheometer equipped with a 40 mm parallel-plate fixture and a 2 mm gap, following the method of (N. Wang et al., 2023). The linear viscoelastic region was determined by a strain sweep from 0.01% to 100% at 1 Hz. Frequency sweeps were subsequently conducted from 0.1 to 100 Hz at 1.0% strain and 25 °C. The storage modulus (G′), loss modulus (G″), and loss tangent (tan δ = G″/G′) were recorded. All measurements were performed in triplicate.

2.6 SEM

The freeze-dried samples were mounted on the sample stage using conductive adhesive and sputter-coated with gold (current: 15 mA, time: 60 s). The microstructure of the samples was observed using a tabletop scanning electron microscope (TM4000, Hitachi, Japan) at an accelerating voltage of 5 kV in backscattered electron (BSE) mode (Ma et al., 2025a).

2.7 Sulfhydryl (S-H) and Disulfide bond (S-S) content

The first step is to dissolve 10.4 g of Tris base, 6.4 g of glycine, and 1.2 g of EDTA in distilled water. The pH of this mixture should then be adjusted to 8.0 using 0.1 mol/L hydrochloric acid, after which it should be diluted to a final volume of 1 L. Ellman's reagent (Solution 2) is prepared by dissolving 40 mg of DTNB in 10 mL of Solution 1. Solution 3 is prepared by mixing 120.12 g of carbamate and 119.413 g of guanidine hydrochloride with Solution 1, after which the volume should be adjusted to 250 mL.

Weigh 75 mg of the sample powder and combine it with 2 mL of Solution 1 and 4.7 g of guanidine hydrochloride. Adjust the resulting mixture to a final volume of 10 mL. Next, pipette 1 mL of this prepared sample dispersion into a 10 mL centrifuge tube. Add 4 mL of Solution 3, followed by 0.05 mL of Solution 2, then measure the absorbance of the mixture at a wavelength of 412 nm (Yue et al., 2025a).

$$SH(\mu mol/g)=73.53A_{412}\times D/C$$

$$S\text{-}S=\frac{-SH_T--SH_F}{2}$$

Where: A_{412} is the absorbance of the sample at 412 nm, D is the dilution factor, the contents of $-SH_F$ and $-SH_T$ are 5.02 and 10, respectively, and C is the sample concentration (mg/mL).

2.8 FT-IR

The freeze-dried sample powder is to be mixed with potassium bromide in a mass ratio of 1:100 (sample:potassium bromide). The mixture is then to be pressed into thin sheets. The instrument parameters were set as follows: the spectral wavenumber range was 4000-400 cm^{-1}, and the number of continuous scans was 64. The absorption peak corresponding to the amide I region (1600-1700 cm^{-1}) was isolated using the OMNIC 8.0 software package, and the spectral data were further processed using Peak Fit software (Ma et al., 2025b).

2.9 Raman spectroscopy

The microenvironment of aromatic amino acids and the conformation of disulfide bonds in gluten were characterised using a Raman spectrometer (XploRA ONE, HORIBA JOBIN YVON SAS, France). Freeze-dried sample powder was

placed on a stainless steel sample stage and irradiated with a 1064 nm laser to acquire spectra. The following detection conditions were used: a spectral range of 400-4000 cm^{-1}, 800 scans, and a resolution of 4 cm^{-1} (Liang et al., 2025).

2.10 Determination of intermolecular forces

Four types of solutions (S1, S2, S3, and S4) were prepared by adding specific components to a phosphate buffer solution (0.05 mol/L, pH 7) as the base solution. S1 contained 0.05 mol/L sodium chloride, S2 contained 0.6 mol/L sodium chloride, S3 contained 0.6 mol/L sodium chloride and 8 mol/L urea; and S4 contained 0.6 mol/L sodium chloride, 8 mol/L urea, and 2% SDS. Weighed samples of 0.2 g were dissolved in 10 mL of each of the four solutions. Following thorough vortex mixing, the mixtures were placed in a constant-temperature water bath shaker and incubated at 25°C with shaking at 180 rpm for 2 h. Subsequent to this, the samples were subjected to centrifugation at low temperature (10000 g, 20 min, 4°C). The sample was collected and 0.5 mL of Coomassie Brilliant Blue reagent was added. Absorbance was measured at a wavelength of 595 nm within a 15 min frame. A standard curve was generated using bovine serum albumin, and the soluble protein content was expressed as milligrams per gram (Q. Wang et al., 2026a).

The difference between S1 and S2 reflects the strength of the ionic bond. The difference between S3 and S2 indicates the strength of hydrogen bonds. The difference between S4 and S3 represents the strength of hydrophobic interactions.

2.11 Circular dichroism analysis

Dissolve a sample solution with a protein concentration of 0.2 mg/mL in

deionized water and place it in a quartz cuvette with a path length of 0.1 cm; under conditions of 25°C and continuous nitrogen purging, scan three times in the wavelength range of 180-260 nm. Detection parameters: bandwidth 1.0 nm, wavelength step 1.0 nm, single-point acquisition time 0.25 s. The final spectrum is the average of the three scans, and baseline correction is performed by subtracting the background spectrum.

2.12 In vitro static gastrointestinal digestion of proteins

The in vitro protein digestion assay was performed with slight modifications based on the method described by Chen et al. (Q. Chen et al., 2025a). Weigh 1.0 g of the WEAX-gluten composite sample, then mix it with 4 ml of distilled water. The mixture was thoroughly homogenized to obtain a uniform sample suspension and was subsequently subjected to sequential simulated gastric and intestinal digestion. The prepared sample was mixed with an equal volume of simulated gastric fluid (SGF), and the pH was adjusted to 3.0. The mixture was incubated at 37°C with shaking for 120 min. After gastric digestion, the pH was adjusted to 7, and an equal volume of simulated intestinal fluid (SIF) was subsequently added. The mixture was further incubated at 37°C with shaking for 120 min. At the end of intestinal digestion, the samples were heated in a boiling-water bath for 15 min to terminate enzymatic hydrolysis and then centrifuged at 5440 × g for 20 min. The supernatant was collected for determination of soluble protein content.

The soluble protein content was determined using a BCA protein quantification kit (Beisheng Biotechnology Co., Ltd., Beijing, China). Briefly, 125 μL of digestion

supernatant was mixed with 1000 μL of BCA working solution in a 2 mL centrifuge tube. The mixture was thoroughly mixed and incubated at 37°C for 30 min, followed by cooling to room temperature. The absorbance was measured at 562 nm using a UV-visible spectrophotometer, and the protein concentration was calculated based on a standard curve prepared using bovine serum albumin (BSA) as the standard. Protein digestibility was calculated using the following equation:

$$\text{Protein digestibility (\%)} = \left(\frac{\text{Protein content in the digestate}}{\text{Protein content in the initial sample}}\right) \times 100\%$$

Where the protein content in the digestate represents the soluble protein content determined in the digestion supernatant, and the protein content in the initial sample represents the protein content of the sample before digestion.

2.13 Statistical analysis

All data resulting from this experiment were obtained from three independent replicates and are presented as mean ± standard deviation. The statistical analysis was conducted using SPSS software. The analysis of variance (ANOVA) model, in conjunction with the Duncan multiple range test, was employed to evaluate the statistical significance of differences in mean values among the groups. A *P*-value less than 0.05 was considered to indicate statistical significance.

3. Results and discussion

3.1 Texture Analysis

The textural properties of gluten proteins are closely related to the integrity of the protein network. Hardness reflects the resistance of the gluten system to

deformation and is generally associated with protein cross-linking and network compactness, whereas springiness reflects the ability of the network to recover after deformation (Y. Yang et al., 2025).

As shown in Fig. 1A and Table 1, AX-0s exhibited significantly lower hardness than Con, reaching 148.96 ± 11.05 g. This reduction suggests that WEAX incorporation altered gluten network organization, possibly through hydration and steric effects that reduced direct protein–protein association. WEAX hydroxyl groups may also participate in hydrogen bonding with gluten proteins, contributing to the redistribution of intermolecular contacts (Zhu et al., 2017a). The relatively high arabinose-to-xylose (A/X) ratio of 0.87 indicates substantial arabinose substitution, which may influence WEAX chain conformation and its interactions within the gluten matrix. These observations are consistent with previous reports that arabinoxylan–protein interactions can modify gluten network organization and mechanical properties (F. Li et al., 2024a).

With increasing ultrasonication time, hardness increased numerically to 197.77 ± 18.08 g at 20 s and then decreased to 178.30 ± 20.32 g at 40 s. This pattern may reflect treatment-dependent reorganization of the WEAX-gluten network through cavitation and mechanical shear. Changes in WEAX distribution and gluten conformation may facilitate component association, contributing to the more compact structure described by SEM at 20 s. Possible WEAX depolymerization could also reduce steric hindrance, although molecular-weight changes were not measured. Continued cavitation and shear at longer durations may disrupt network continuity,

284 contributing to the numerical decrease in hardness at 40 s (Kong et al., 2023; T. Wang
285 et al., 2026).

286 Springiness exhibited a response distinct from that of hardness. AX-0s showed
287 greater springiness than Con, and the value increased numerically to 0.94 ± 0.01 after
288 40 s of ultrasonication. WEAX-associated hydration and reversible intermolecular
289 interactions may contribute to the recovery of the composite network following
290 compression (H. Li et al., 2026). In addition, ultrasonic degradation and redistribution
291 of WEAX may reduce its molecular weight and increase its mobility, thereby
292 alleviating the disruptive effect of high-molecular-weight WEAX and promoting the
293 viscoelasticity of the gluten network (Zhao et al., 2025).

294 **3.2 Rheological properties**

295 The storage modulus (G′), loss modulus (G″), and loss tangent (tan δ = G″/G′)
296 were used to characterize the viscoelastic behavior of the WEAX–gluten composites.
297 G′ represents elastic energy storage, whereas G″ reflects viscous energy dissipation. A
298 tan δ below 1 indicates an elastic-dominated response under the measurement
299 conditions (Zhao et al., 2024).

300 As shown in Fig. 1B, AX-0s exhibited a pronounced frequency-dependent
301 increase in G′ and the highest values at higher frequencies. WEAX-associated water
302 binding and space-filling effects may modify hydration and restrict molecular
303 mobility within the gluten matrix, contributing to increased elastic stiffness (X. Guo et
304 al., 2018). At higher frequencies, sonicated composites exhibited lower G′ than AX-0s
305 but remained above Con, with AX-10s showing the highest G′ and AX-40s the lowest

306 among the sonicated groups. These responses suggest that ultrasonication modified
307 the elastic contribution of the composite through changes in WEAX distribution and
308 protein association (Yue et al., 2025b).

309 G″ represents the energy dissipated as heat during deformation and reflects the
310 viscous behavior of the composite system. As shown in Fig. 1C, AX-0s exhibited a
311 lower G″ than Con, indicating a more elastic-dominated response after WEAX
312 incorporation. The interpenetrating WEAX-gluten network restricted protein-chain
313 rearrangement and reduced molecular friction during deformation, thereby decreasing
314 viscous energy dissipation (Pietiäinen et al., 2024). After ultrasonic treatment, G″ was
315 larger compared to AX-0s, among them, the largest one is AX-30s, then AX-10s and
316 AX-40s. The ultrasonic degradation reduced length of WEAX chains and enhanced its
317 molecular mobility which increases molecular friction upon deformation and
318 enhances viscous energy dissipation (Ahmed et al., 2024). Following ultrasonic
319 treatment, G″ values were generally higher than that of AX-0s, with AX-30s showing
320 the highest value. However, prolonged ultrasonication caused further WEAX
321 degradation and reduced its molecular size, weakening intermolecular friction and
322 viscous energy dissipation, which ultimately lowered G″ at 40 s.

323 Loss tangent ($\tan\delta = G''/G'$), represents the ratio between viscous vs elastic
324 behavior in the viscoelastic response. The Con group had the largest $\tan\delta$ over all
325 tested frequencies (>1 for high frequencies), implying larger viscous contribution
326 during high-frequency deformations, whereas AX-0s have the smallest $\tan\delta$
327 decreasing as frequency increases, implying that incorporating WEAX increased

elasticity and structural stability of the composite network (L. Li et al., 2016). Ultrasonic treatment increased tanδ relative to AX-0s, indicating a shift toward a greater viscous contribution in the composite system, although the values remained below that of Con. Among the ultrasonicated groups, AX-20s showed a relatively lower tanδ, suggesting a comparatively greater elastic contribution. Prolonged ultrasonication may have reduced the molecular size and altered the distribution of WEAX, weakening its noncovalent interactions with gluten and reducing its elastic support. Consequently, the elastic contribution decreased while the relative viscous contribution increased (Y. Liu et al., 2020).

3.3 Microstructure of the WEAX-gluten complex

SEM images (200 ×, scale bar = 200 μm) clearly demonstrated that there were significant differences on pore distribution, framework thickness, and structural continuity for the gluten network after incorporating WEAX and ultrasonic treatment (Fig. 2A). The Con had a relatively thin and uneven protein framework with irregular pores and local fractures due to its heterogeneous gluten network. For AX-0s, it has a loose honeycomb structure with many small pores. It is likely because of the water binding effect and steric interference from WEAX interferes directly with protein–protein association and modifies gluten aggregation (M. Liu et al., 2021b). The gluten network at 10 s (AX-10s) was finer, having thick protein strands, large pores, and better continuity; moderate cavitation might lead to a partial unfolding of proteins and WEAX-gluten interactions. The network at 20 s (AX-20s) was denser and more uniform, containing regular pores and good continuity without visible fractures, these

could be due to moderate protein rearrangement and increased noncovalent interactions in the WEAX-gluten network (Z. Guo et al., 2021).

At 30 s (AX-30s), the WEAX-gluten network showed obvious structural deterioration, with a thinner and partially fractured protein framework, irregular pores, and reduced continuity. At 40 s (AX-40s), this deterioration became more pronounced, with extensive framework fragmentation and irregular cavities. Prolonged cavitation and shear may have further degraded WEAX and disrupted its interactions with gluten, while also perturbing disulfide and hydrophobic interactions within the protein network, thereby weakening the structural integrity of the composite network (J. Wang et al., 2024). The above mentioned microstructural changes correlate well with our textural results in Section 3.1 where prolonged ultrasonication decreased network hardness from 197.77 ± 18.08 g (20 s) to 178.30 ± 20.32 g (40 s) but increased its springiness from 0.88 ± 0.01 to 0.94 ± 0.01 which verifies that the structure is disordered and has changed viscoelastic properties for the over-treated gluten system.

In summary, Prolonged ultrasonic treatment causes dynamic microstructure change within the gluten protein-AX composite system, comprising three phases (initial structural adjustment phase; subsequent repair and optimization phase; finally structural degradation phase). The microstructural evolution is well correlated with the macroscopic variation measured from texture analysis or rheology. Our results confirm that moderate ultrasonic treatment optimizes the microscopic network architecture through modulation of the conformational behavior of AX molecules and

promotion of order cross-linking between AX and gluten proteins, fundamentally improving the macroscopic functional properties of the composite system.

3.4 Sulfhydryl (S-H) and disulfide bond (S-S) content

The primary covalent bonds that maintain the three-dimensional network structure of gluten proteins are -SH and S-S. The dynamic transformation of these bonds directly affects the cross-linking strength and conformational stability between protein molecules (R.-X. Wang et al., 2023).

As shown in Fig. 2B, disulfide content decreased by 49.45% in AX-0s compared with Con. WEAX-associated steric effects and changes in hydration may alter direct protein–protein association, thereby influencing disulfide cross-linking (Sun et al., 2022). Ultrasonication further reduced disulfide content, which reached its minimum at 20 s, corresponding to a 65.38% reduction relative to Con. Ultrasound-induced WEAX redistribution and gluten conformational rearrangement may contribute to these changes. Notably, the lowest disulfide content coincided with the highest numerical hardness and the compact microstructure observed at 20 s. This suggests that hardness depended on the overall organization of the composite network, with changes in protein conformation and noncovalent association potentially contributing alongside disulfide cross-linking (F. Li et al., 2024a).

Sulfhydryl content was numerically higher in WEAX-containing samples than in Con, increased to a maximum at 10 s, and subsequently declined, although differences among groups were not significant ($p > 0.05$). WEAX-mediated steric effects may reduce direct gluten–gluten contact and limit the oxidation of sulfhydryl

groups to disulfide bonds (F. Li et al., 2023). During early ultrasonication, cavitation and mechanical shear may promote gluten-chain rearrangement and expose previously buried thiol groups, contributing to the numerical increase at 10 s (Y. Wang et al., 2023a). The subsequent decline in -SH content may reflect -SH reassociation or changes in -SH accessibility during continued protein rearrangement.

3.5 Secondary structural transformation revealed by FT-IR spectroscopy

Changes in the relative proportions of α-helices, β-sheets, β-turns, and random coils provide information on gluten conformational rearrangement during WEAX incorporation and ultrasonication (Hong et al., 2024).

As shown in Fig. 2C, AX-0s exhibited lower α-helix and β-sheet contents than Con, reaching 14.09% and 19.71%, respectively, accompanied by an increase in β-turn content to 54.44%. WEAX-associated steric effects and noncovalent interactions may modify protein association and conformational organization (Zhu et al., 2019). These changes accompanied the reduced S-S content and looser microstructure observed in AX-0s.

At 10 s, α-helix and β-sheet contents increased to 20.80% and 26.28%, respectively, while β-turn and random-coil contents were 36.77% and 16.14%. This redistribution suggests ultrasound-induced gluten-chain rearrangement (J. Zhang et al., 2021a).

At 20 s, β-sheet content reached its highest numerical value of 26.93%, with α-helix, random-coil, and β-turn contents of 18.03%, 15.94%, and 39.10%, respectively. WEAX redistribution may facilitate protein–polysaccharide contact and

contribute to conformational rearrangement through noncovalent association (P. Wang, Zhao, et al., 2020).

At 30 and 40 s, β-sheet contents were 26.80% and 26.32%, α-helix contents were 16.42% and 16.82%, and β-turn contents were 41.67% and 41.51%, respectively. Differences in β-sheet content among sonicated groups were not significant. These responses therefore indicate continued redistribution of secondary-structure components rather than a pronounced loss of β-sheet structure. Together with the SEM observations, they suggest that prolonged ultrasonication modified both protein conformation and composite network organization (Y. Wang et al., 2023b).

Two-dimensional correlation spectroscopy (2D-COS) was used to examine treatment-dependent spectral responses in the 1200–1700 and 2700–3400 cm^{-1} regions (Peng et al., 2025).The synchronous spectrum in Fig. 2D showed prominent correlation features near 1400 cm^{-1} and within the amide I region, indicating changes in protein-associated vibrational environments. The 1200–1500 cm^{-1} region contains overlapping contributions from protein and polysaccharide groups, which may contribute to the observed spectral responses (S. Yang et al., 2022).

In the synchronous spectrum (Fig. 2D), prominent diagonal autopeaks occurred in the amide I region (1600-1700 cm^{-1}) and around 1400 cm^{-1}, indicating treatment-dependent changes in peptide-backbone and side-chain-associated vibrational environments. The region around 1400 cm^{-1} may also contain overlapping polysaccharide contributions. The 1500-1600 cm^{-1} region, including the amide II band near 1550 cm^{-1}, showed relatively lower correlation intensity. These features suggest

437 that the associated vibrational groups exhibited different magnitudes of response to
438 ultrasonication, consistent with changes in protein conformation and the local
439 interaction environment of the WEAX-gluten composite.

440 The synchronous spectrum (Fig. 2E) showed stronger correlation intensities in
441 the 3200-3400 cm^{-1} region than in the 2700-3000 cm^{-1} region, which are associated
442 mainly with O-H/N-H and C-H stretching vibrations, respectively. The greater
443 response of O-H/N-H-associated bands may reflect changes in hydration and the
444 hydrogen-bonding environment during ultrasonication, consistent with previously
445 reported conformational rearrangement of gluten proteins (J. Zhang et al., 2021b).
446 The predominance of positive cross-peaks indicates similarly directed changes in
447 spectral intensity at the corresponding coordinates, suggesting coordinated vibrational
448 responses during structural reorganization of the WEAX–gluten composite.

449 The asynchronous spectrum (Fig. 2F) showed cross-peaks between the
450 α-helix-associated region (1652-1660 cm^{-1}) and the β-sheet (1605-1640 cm^{-1}) and
451 random-coil (1640-1652 cm^{-1}) regions, indicating non-synchronous changes in the
452 corresponding spectral intensities. Asynchronous correlations were also observed
453 between the 1200-1400 cm^{-1} region, which includes overlapping polysaccharide and
454 protein contributions, and the amide I region. These spectral responses suggest that
455 the associated vibrational groups responded differently during ultrasonication,
456 consistent with conformational rearrangement within the WEAX-gluten composite.

457 The asynchronous spectrum (Fig. 2G) showed cross-peaks between the O-H/N-H
458 stretching region near 3300 cm^{-1} and the C-H stretching region near 2900 cm^{-1},

indicating non-synchronous changes in the corresponding spectral intensities. WEAX may interact with gluten proteins through hydrogen bonding, thereby modifying the local interaction environment (Zhu et al., 2017b). Ultrasound-induced changes in hydrogen bonding have also been associated with gluten conformational rearrangement (J. Zhang et al., 2021c). Together with the amide-region responses, these spectral features suggest that changes in the hydrogen-bonding environment accompanied protein conformational rearrangement during ultrasonication of the WEAX-gluten composite.

3.6 Circular dichroism (CD)

Circular dichroism (CD) spectroscopy provides information on protein secondary structure through changes in spectral shape and intensity (Ding et al., 2026).

As shown in Fig. 3A, all samples exhibited a positive band near 190 nm and a negative band at approximately 208–210 nm, while no clearly resolved negative band was observed near 222 nm. AX-0s exhibited changes in spectral intensity relative to Con, suggesting an altered gluten conformational environment following WEAX incorporation (Zhou et al., 2021). The amplitudes of the positive and negative bands generally increased with ultrasonication time, with AX-40s showing the most pronounced response. Cavitation and mechanical shear may promote gluten-chain unfolding and rearrangement, contributing to these spectral changes (H. Cao et al., 2021).

The CD responses were consistent with the redistribution of secondary-structure components detected by FTIR. WEAX incorporation decreased α-helix and β-sheet

contents and increased β-turn content, whereas subsequent ultrasonication induced further treatment-dependent changes in their proportions. The combined CD and FTIR results therefore suggest that WEAX incorporation and ultrasonication modified the conformational organization of gluten proteins within the composite.

3.7 Regulation of the tertiary structure of the WEAX-gluten composite system by ultrasound

Raman spectroscopy provides information on aromatic amino acid microenvironments and disulfide conformations, allowing characterization of local conformational changes in gluten proteins (Lancelot et al., 2021a).

The I_{755} index decreased numerically from 1.194 ± 0.005 in Con to 1.187 ± 0.006 in AX-0s and 1.183 ± 0.004 at 10 s, followed by an increase to 1.191 ± 0.001 at 40 s (Table 2). Although differences among groups were not significant, this numerical pattern may reflect local changes in the Trp microenvironment during WEAX incorporation and ultrasonication (P. Wang, Zou, et al., 2020). WEAX-associated changes in protein association and ultrasound-induced chain rearrangement may contribute to these responses (F. Li et al., 2024b).

The Tyr doublet ratio, I_{850}/I_{830}, provides information on the local hydrogen-bonding environment of Tyr residues (Lancelot et al., 2021b). Values ranged from 0.946 to 0.949, with no significant differences among groups ($p > 0.05$), indicating limited variation in this Tyr-associated spectral index.

Disulfide stretching bands were assigned to gauche–gauche–gauche (g-g-g), trans-gauche-gauche (t-g-g), and trans-gauche-trans (t-g-t) conformations. Their

503 relative proportions reflect the local conformational environment of S-S bonds (P.
504 Wang et al., 2022). The t-g-g and t-g-t proportions ranged from 27.84% to 28.42%
505 and from 54.20% to 56.09%, respectively, with no significant differences among
506 groups ($p > 0.05$). Thus, t-g-t remained the predominant fitted conformation
507 throughout treatment.

508 The g-g-g proportion decreased from 17.70 ± 0.65% in Con to 16.65 ± 0.42% in
509 AX-0s and reached its minimum of 15.78 ± 0.64% at 10 s, which was significantly
510 lower than Con ($p < 0.05$). Values subsequently recovered numerically to 16.55 ±
511 0.02%, 17.46 ± 1.14%, and 17.38 ± 0.54% at 20, 30, and 40 s, respectively.
512 WEAX-associated steric effects and ultrasound-induced protein rearrangement may
513 modify the local S-S environment, contributing to this nonmonotonic response (W.
514 Chen et al., 2022). Together with the aromatic-residue indices, these findings suggest
515 localized conformational rearrangement within the WEAX-gluten composite.

516 **3.8 Intermolecular forces**

517 Noncovalent interactions, including hydrogen bonding, hydrophobic interactions,
518 and ionic interactions, contribute to gluten network organization and stability (Q.
519 Wang et al., 2026b).

520 The hydrogen-bonding-related fraction did not differ significantly between Con
521 and any WEAX-containing group ($p > 0.05$, Fig. 3B). AX-0s exhibited a value of 7.27
522 ± 1.92 mg/g, which decreased numerically to a minimum of 5.89 ± 0.66 mg/g at 20 s,
523 followed by partial recovery at 30 and 40 s. WEAX hydroxyl groups may participate
524 in hydrogen bonding with gluten proteins and modify hydration within the composite.

525 Ultrasound-induced protein rearrangement and WEAX redistribution may further
526 modify existing hydrogen-bonding contacts, contributing to the observed numerical
527 variation (F. Li et al., 2024c; J. Zhang et al., 2021d).

528 The hydrophobic interaction-related fraction showed a nonmonotonic response
529 (Fig. 3C). AX-0s did not differ significantly from Con ($p > 0.05$), which exhibited a
530 value of 85.65 ± 2.35 mg/g. AX-10s showed a significantly higher value of 93.20 ±
531 2.43 mg/g than Con ($p < 0.01$), whereas AX-20s and AX-30s exhibited significantly
532 lower values ($p < 0.001$). The fraction recovered numerically after 20 s, reaching
533 86.04 ± 2.03 mg/g at 40 s, AX-40s also differed significantly from Con ($p < 0.01$).
534 The initial increase may reflect protein-chain rearrangement and changes in
535 hydrophobic contacts. Continued ultrasonication may reorganize protein aggregates
536 and redistribute these contacts, contributing to the subsequent decrease and recovery
537 (Q. Wang et al., 2026c).

538 The ionic interaction-related fraction was significantly higher in all
539 WEAX-containing groups than in Con (Fig. 3D). AX-0s exhibited a value of 4.11 ±
540 0.34 mg/g compared with 1.62 ± 0.70 mg/g in Con ($p < 0.01$). The sonicated groups
541 also exceeded Con, with differences at $p < 0.05$ for AX-10s, $p < 0.01$ for AX-20s and
542 AX-30s, and $p < 0.001$ for AX-40s. Among sonicated composites, the fraction
543 reached a numerical minimum of 3.42 ± 0.85 mg/g at 20 s and a maximum of 5.03 ±
544 0.81 mg/g at 40 s. WEAX-associated hydration and ultrasound-induced
545 conformational rearrangement may alter the accessibility and distribution of charged

546 protein groups, contributing to changes in charge-mediated associations within the
547 composite (G. Cao et al., 2026).

548 **3.9 In vitro static digestion of proteins**

549 Protein network organization and substrate accessibility to digestive enzymes are
550 important factors influencing the digestive behavior of gluten composites (Q. Chen et
551 al., 2025b).

552 As shown in Fig. 4A, all WEAX-containing groups exhibited significantly lower
553 gastric apparent digestibility than Con ($p < 0.0001$). WEAX incorporation reduced the
554 value from 41.82 ± 1.48% in Con to 27.47 ± 1.03% in AX-0s. Gastric apparent
555 digestibility decreased further numerically at 10 s, subsequently increased to its
556 highest value among sonicated composites at 30 s (32.48 ± 0.60%), and declined at 40
557 s. Thus, treatment for 20-40 s partly alleviated the WEAX-associated reduction,
558 although values remained below Con.

559 WEAX-associated hydration and steric effects may restrict contact between
560 pepsin and gluten proteins, contributing to the reduced gastric apparent digestibility.
561 The further numerical decrease at 10 s may reflect changes in protein–polysaccharide
562 association during initial structural rearrangement. With longer treatment, WEAX
563 redistribution and gluten conformational changes may improve enzyme accessibility,
564 contributing to the higher values at 20-30 s. The subsequent numerical decline at 40 s
565 may be associated with further rearrangement of gluten proteins and redistribution of
566 intermolecular interactions within the WEAX-gluten network (Q. Chen et al., 2025c).

As shown in Fig. 4B, none of the WEAX-containing groups differed significantly from Con in intestinal apparent digestibility ($p > 0.05$). Con and AX-0s exhibited values of 56.69 ± 2.14% and 57.85 ± 0.17%, respectively. Values fluctuated numerically with ultrasonication time, reaching a minimum of 52.83 ± 2.96% at 30 s and recovering to 56.07 ± 0.73% at 40 s. Differences associated with WEAX incorporation and ultrasonication were less pronounced during intestinal digestion than during the gastric phase.

The different intestinal response may be related to changes in protein–polysaccharide associations under intestinal digestion conditions and continued enzymatic hydrolysis of gluten proteins. Ultrasound-induced changes in protein conformation and intermolecular interactions may contribute to the numerical variation among groups (Yu et al., 2023). The recovery at 40 s may also be associated with the greater network fragmentation observed by SEM. Together, these findings suggest that WEAX incorporation and ultrasonication affected gastric and intestinal digestion differently, with relatively small differences in the intestinal endpoint (Cheng et al., 2024).

In summary, WEAX incorporation reduced gastric apparent digestibility but had a limited effect on intestinal apparent digestibility. Ultrasonication partly alleviated the WEAX-associated reduction in gastric apparent digestibility, potentially through WEAX degradation and reorganization of the composite network. Gastric apparent digestibility reached its highest numerical value among the WEAX-containing groups at 30 s, whereas intestinal apparent digestibility did not differ significantly from that

of Con. These findings suggest that WEAX incorporation and ultrasonication exerted different effects on gastric and intestinal digestion, providing a potential approach for modifying the digestive properties of wheat gluten.

3.10 Potential mechanisms underlying the effects of ultrasound on the digestion characteristics of WEAX protein complexes

Pearson correlation analysis and principal component analysis (PCA) were performed to characterize the relationships among protein conformation, intermolecular interactions, textural properties, and digestibility in the WEAX-gluten composite system. The results are presented in Fig. 5A and 5B.

Pearson correlation analysis revealed associations among structural, textural, and digestive parameters (Fig. 5A). Hardness correlated positively with β-sheet content ($r = 0.58$) and negatively with the hydrophobic interaction-related fraction ($r = -0.67$), whereas its correlations with disulfide content and the ionic interaction-related fraction were weak. Springiness correlated positively with the ionic interaction-related fraction ($r = 0.80$). Intestinal apparent digestibility correlated positively with disulfide content ($r = 0.84$) and I_{755} ($r = 0.69$), but showed a weaker correlation with β-sheet content ($r = 0.27$). These associations suggest that textural and digestive properties were related to different aspects of protein conformation and intermolecular association.

PC1 and PC2 explained 38.6% and 23.7% of the total variance, respectively, accounting for 62.3% in combination (Fig. 5B). Partial overlap among the 20-40 s groups indicated similar multivariate characteristics despite differences in individual

parameters. PCA therefore complemented the specific associations identified by Pearson correlation analysis.

At 20 s, the highest numerical hardness coincided with a β-sheet content of 26.93%, the lowest disulfide content, and a compact network observed by SEM. At 40 s, the ionic interaction-related fraction reached its maximum, whereas hardness decreased numerically and network fragmentation became more pronounced. These responses suggest that hardness was associated with the combined organization of protein conformation and intermolecular interactions. Gastric apparent digestibility reached its highest numerical value among WEAX-containing groups at 30 s, indicating that texture and digestion responded differently to ultrasonication duration.

As illustrated in Fig. 6, WEAX-associated hydration, steric effects, and noncovalent interactions may initially modify gluten association. Subsequent ultrasonication may promote WEAX redistribution, possible WEAX degradation, and gluten conformational rearrangement, contributing to network reorganization at moderate durations and reduced structural continuity during prolonged ultrasonication. These changes may influence gluten proteolysis, contributing to the different gastric and intestinal responses. Overall, the proposed mechanism links the observed textural and digestive changes to the dynamic reorganization of protein conformation and intermolecular interactions within the WEAX–gluten composite.

4. Conclusion

This study investigated the effects of wastewater-recovered WEAX and oscillating-plate ultrasonication on the structural, textural, and digestive properties of

wheat gluten. WEAX incorporation decreased hardness, increased springiness, and reduced gastric apparent digestibility, accompanied by changes in protein conformation, disulfide content, and noncovalent interactions. Ultrasonication induced duration-dependent reorganization of the WEAX-gluten network. At 20 s, the highest numerical hardness coincided with a compact microstructure despite reduced disulfide content. Prolonged ultrasonication was accompanied by greater network fragmentation and a numerical decrease in hardness. Ultrasonication partly alleviated the WEAX-associated reduction in gastric apparent digestibility, which reached its highest numerical value among WEAX-containing groups at 30 s (32.48 ± 0.60%) but remained below that of Con. Intestinal apparent digestibility showed numerical variation, with a minimum at 30 s and recovery at 40 s, differences from Con were not significant. Overall, these findings suggest that the textural and digestive responses involved coordinated changes in gluten conformation, intermolecular interactions, and network organization. They provide a basis for modifying wheat gluten properties through WEAX incorporation and ultrasonication and support the potential valorization of WEAX recovered from wheat gluten processing wastewater.

Menglong Liu: Writing - original draft, Resources, Methodology, Investigation, Formal analysis, Data curation, Conceptualization. **Shaokai Wang**: Resources, Project administration. **Hongyan Li**: Resources, Project administration, Investigation. **Yuanyuan Chen**: Supervision, Investigation, Conceptualization. **Chonghui Yue**: Visualization, Supervision, Software, Conceptualization. **Peiyan L**i: Resources, Project administration. **Denglin Luo**: Visualization, Supervision. **Jinying Guo**:

Writing – review & editing, Project administration, Conceptualization. **Zhouya Bai**: Writing - review & editing, Project administration, Funding acquisition, Conceptualization.

Declaration of competing interest

The authors declare no conflict of interest.

Data availability

Data will be made available on request.

Acknowledgments

This study was supported by the financial support from Henan Province Science and Technology Research Projects (242102110129), Henan Provincial Joint Fund Cultivation Project (252301420060), National Natural Science Foundation Youth Fund (32302075), Henan Province College Students' Innovation and Entrepreneurship Training Program (202610464035)

673 **References**

674 Ahmed, Z., Xu, B., Farooq, U., Manzoor, M. F., Awad, M. F., Ashraf, J., Tufail, T., &
675 Abdi, G. (2024). Impact of multi-frequency ultrasound processing with
676 different treatment times on the structural quality of frozen wheat dough.
677 Ultrasonics Sonochemistry, 111, 107116.
678 https://doi.org/10.1016/j.ultsonch.2024.107116
679 Bai, Z., Wan, J., Deng, W., Wang, Y., Chen, Y., Li, P., Yue, C., & Luo, D. (2026a).
680 Mechanism of ultrasound-modulated gluten-inulin interactions: Impact of
681 inulin polymerization degree. Food Research International, 233, 118963.
682 https://doi.org/10.1016/j.foodres.2026.118963
683 Bai, Z., Wan, J., Deng, W., Wang, Y., Chen, Y., Li, P., Yue, C., & Luo, D. (2026b).
684 Mechanism of ultrasound-modulated gluten-inulin interactions: Impact of
685 inulin polymerization degree. Food Research International, 233, 118963.
686 https://doi.org/10.1016/j.foodres.2026.118963
687 Cao, G., Yang, Z., Li, X., He, X., Song, S., & Wen, C. (2026). The combined effects
688 of konjac glucomannan and ultrasound treatments on the interaction of gluten
689 and surimi protein. Food Chemistry: X, 33, 103492.
690 https://doi.org/10.1016/j.fochx.2026.103492
691 Cao, H., Sun, R., Shi, J., Li, M., Guan, X., Liu, J., Huang, K., & Zhang, Y. (2021).
692 Effect of ultrasonic on the structure and quality characteristics of quinoa
693 protein oxidation aggregates. Ultrasonics Sonochemistry, 77, 105685.
694 https://doi.org/10.1016/j.ultsonch.2021.105685

Chen, Q., Ji, H., Wang, Z., Wang, Y., Wang, X., & Chen, Z. (2025a). Effects of different charged polysaccharides on the gelation properties and in vitro digestibility of potato protein gel: Insight into underlying mechanisms. Food Hydrocolloids, 164, 111187. https://doi.org/10.1016/j.foodhyd.2025.111187

Chen, Q., Ji, H., Wang, Z., Wang, Y., Wang, X., & Chen, Z. (2025b). Effects of different charged polysaccharides on the gelation properties and in vitro digestibility of potato protein gel: Insight into underlying mechanisms. Food Hydrocolloids, 164, 111187. https://doi.org/10.1016/j.foodhyd.2025.111187

Chen, Q., Ji, H., Wang, Z., Wang, Y., Wang, X., & Chen, Z. (2025c). Effects of different charged polysaccharides on the gelation properties and in vitro digestibility of potato protein gel: Insight into underlying mechanisms. Food Hydrocolloids, 164, 111187. https://doi.org/10.1016/j.foodhyd.2025.111187

Chen, W., Ma, H., & Wang, Y.-Y. (2022). Recent advances in modified food proteins by high intensity ultrasound for enhancing functionality: Potential mechanisms, combination with other methods, equipment innovations and future directions. Ultrasonics Sonochemistry, 85, 105993. https://doi.org/10.1016/j.ultsonch.2022.105993

Cheng, Y., Shi, X., Yeboah, G. B., Chen, L., & Wu, J. (2024). Effect of Multi-Mode Divergent Ultrasound Pretreatment on Hardness, Microstructure and Digestion of Acid-Induced Whey Protein Gels. Foods, 13(12), 1926. https://doi.org/10.3390/foods13121926

716 Ding, Y., Ettelaie, R., Zhang, K., & Wang, L. (2026). Synergistic modification of soy
717 protein as plant-based molecular emulsifiers by enzymatic hydrolysis and
718 heat-assisted pH shifting. Food Chemistry: X, 34, 103561.
719 https://doi.org/10.1016/j.fochx.2026.103561
720 Geng, M., Li, J., Luo, D., Li, X., Zhang, Y., Lan, H., Huang, J., Bai, Z., & Han, S.
721 (2024). Recycling of wheat gluten wastewater: Separation, characterisation,
722 and solution rheology of arabinoxylans. International Journal of Food Science
723 & Technology, 59(3), 1852–1863. https://doi.org/10.1111/ijfs.16937
724 Guo, X., Yang, S., & Zhu, K. (2018). Impact of arabinoxylan with different molecular
725 weight on the thermo-mechanical, rheological, water mobility and
726 microstructural characteristics of wheat dough. International Journal of Food
727 Science & Technology, 53(9), 2150–2158. https://doi.org/10.1111/ijfs.13802
728 Guo, Z., Liu, M., Xiang, X., Wang, Z., Yang, B., Chen, X., Chen, G., & Kan, J.
729 (2021). Effects of inulins with various molecular weights and added
730 concentrations on the structural properties and thermal stability of
731 heat-induced gliadin and glutenin gels. LWT, 149, 111891.
732 https://doi.org/10.1016/j.lwt.2021.111891
733 Hong, T., Tan, Z., Yang, T., Xu, D., Jin, Y., Wu, F., & Xu, X. (2024). Dynamic
734 behavior of zein-gluten interaction during extruded noodle processing. Food
735 Hydrocolloids, 147, 109320. https://doi.org/10.1016/j.foodhyd.2023.109320
736 Kong, Y., Sun, L., Wu, Z., Li, Y., Kang, Z., Xie, F., & Yu, D. (2023). Effects of
737 ultrasonic treatment on the structural, functional properties and beany flavor of

soy protein isolate: Comparison with traditional thermal treatment. Ultrasonics Sonochemistry, 101, 106675. https://doi.org/10.1016/j.ultsonch.2023.106675

Lancelot, E., Fontaine, J., Grua-Priol, J., Assaf, A., Thouand, G., & Le-Bail, A. (2021a). Study of structural changes of gluten proteins during bread dough mixing by Raman spectroscopy. Food Chemistry, 358, 129916. https://doi.org/10.1016/j.foodchem.2021.129916

Lancelot, E., Fontaine, J., Grua-Priol, J., Assaf, A., Thouand, G., & Le-Bail, A. (2021b). Study of structural changes of gluten proteins during bread dough mixing by Raman spectroscopy. Food Chemistry, 358, 129916. https://doi.org/10.1016/j.foodchem.2021.129916

Li, F., Li, T., Zhao, J., Fan, M., Qian, H., Li, Y., & Wang, L. (2023). Entanglement between Water Un-Extractable Arabinoxylan and Gliadin or Glutenins Induced a More Fragile and Soft Gluten Network Structure. Foods, 12(9), 1800. https://doi.org/10.3390/foods12091800

Li, F., Li, T., Zhao, J., Fan, M., Qian, H., Li, Y., & Wang, L. (2024a). Unraveling the deterioration mechanism of dough during whole wheat flour processing: A case study of gluten protein containing arabinoxylan with different molecular weights. Food Chemistry, 432, 137199. https://doi.org/10.1016/j.foodchem.2023.137199

Li, F., Li, T., Zhao, J., Fan, M., Qian, H., Li, Y., & Wang, L. (2024b). Unraveling the deterioration mechanism of dough during whole wheat flour processing: A case study of gluten protein containing arabinoxylan with different molecular

760 weights. Food Chemistry, 432, 137199.
761 https://doi.org/10.1016/j.foodchem.2023.137199
762 Li, F., Li, T., Zhao, J., Fan, M., Qian, H., Li, Y., & Wang, L. (2024c). Unraveling the
763 deterioration mechanism of dough during whole wheat flour processing: A
764 case study of gluten protein containing arabinoxylan with different molecular
765 weights. Food Chemistry, 432, 137199.
766 https://doi.org/10.1016/j.foodchem.2023.137199
767 Li, H., He, J., Liu, Y., Liu, X., & Liu, T. (2026). Auricularia auricula Polysaccharide
768 Modulates Rheological, Thermal, and Structural Properties of Wheat Gluten
769 via Selective Regulation of Glutenin and Gliadin. Foods, 15(1), 136.
770 https://doi.org/10.3390/foods15010136
771 Li, L., Ma, S., Fan, L., Zhang, C., Pu, X., Zheng, X., & Wang, X. (2016). The
772 influence of ultrasonic modification on arabinoxylans properties obtained from
773 wheat bran. International Journal of Food Science & Technology, 51(11),
774 2338–2344. https://doi.org/10.1111/ijfs.13239
775 Li, X., Liu, P., Bai, Z., Luo, D., Yue, C., Wu, Y., Li, P., Wang, L., & Han, S. (2024).
776 Ultrasound-assisted process of dough for noodle production: Textural
777 properties, moisture distribution, microstructure and cooking quality. Journal
778 of Cereal Science, 119, 104005. https://doi.org/10.1016/j.jcs.2024.104005
779 Liang, Y., Zhang, P., Liu, H., Liu, M., He, B., & Wang, J. (2025). Impact of
780 fermentation methods on gluten aggregation and structural properties in frozen

cooked fermented hollow noodles during freeze-thaw cycles. Food Chemistry, 477, 143607. https://doi.org/10.1016/j.foodchem.2025.143607

Liu, M., Chen, G., Zhang, H., Yu, Q., Mei, X., & Kan, J. (2021a). Heat-induced inulin-gluten gel: Insights into the influences of inulin molecular weight on the rheological and structural properties of gluten gel to molecular and physicochemical characteristics. Food Hydrocolloids, 111, 106397. https://doi.org/10.1016/j.foodhyd.2020.106397

Liu, M., Chen, G., Zhang, H., Yu, Q., Mei, X., & Kan, J. (2021b). Heat-induced inulin-gluten gel: Insights into the influences of inulin molecular weight on the rheological and structural properties of gluten gel to molecular and physicochemical characteristics. Food Hydrocolloids, 111, 106397. https://doi.org/10.1016/j.foodhyd.2020.106397

Liu, Y., Wang, S., Kang, J., Wang, N., Xiao, M., Li, Z., Wang, C., Guo, Q., & Hu, X. (2020). Arabinoxylan from wheat bran: Molecular degradation and functional investigation. Food Hydrocolloids, 107, 105914. https://doi.org/10.1016/j.foodhyd.2020.105914

Ma, Y., Xu, M., Wang, W., Li, X., & Ding, X. (2025a). Ultrasound assisted complexation of soybean peptide aggregates and soluble soybean polysaccharide: pH optimization, structure characterization, and emulsifying behavior. Food Research International, 201, 115546. https://doi.org/10.1016/j.foodres.2024.115546

802 Ma, Y., Xu, M., Wang, W., Li, X., & Ding, X. (2025b). Ultrasound assisted
803 complexation of soybean peptide aggregates and soluble soybean
804 polysaccharide: pH optimization, structure characterization, and emulsifying
805 behavior. Food Research International, 201, 115546.
806 https://doi.org/10.1016/j.foodres.2024.115546
807 Meng, K., Wang, Q., Luo, D., Bai, Z., Yue, C., & Sun, S. (2026). Effects of array
808 vibrating-plate ultrasound treatment on dough sheets: Macroscopic properties,
809 microstructure, physicochemical and hydration characteristics. Innovative
810 Food Science & Emerging Technologies, 112, 104693.
811 https://doi.org/10.1016/j.ifset.2026.104693
812 Mika, M., & Wikiera, A. (2024). Enzymatic Hydrolysis as an Effective Method for
813 Obtaining Wheat Gluten Hydrolysates Combining Beneficial Functional
814 Properties with Health-Promoting Potential. Molecules, 29(18), 4407.
815 https://doi.org/10.3390/molecules29184407
816 Peng, S., Wang, F., Wei, D., Wang, C., Ma, H., & Du, Y. (2025). Application of FTIR
817 two-dimensional correlation spectroscopy (2D-COS) analysis in characterizing
818 environmental behaviors of microplastics: A systematic review. Journal of
819 Environmental Sciences, 147, 200–216.
820 https://doi.org/10.1016/j.jes.2023.10.004
821 Pietiäinen, S., Lee, Y., Jimenez-Quero, A., Katina, K., Maina, N. H., Hansson, H.,
822 Moldin, A., & Langton, M. (2024). Feruloylation and Hydrolysis of

Arabinoxylan Extracted from Wheat Bran: Effect on Dough Rheology and Microstructure. Foods, 13(15), 2309. https://doi.org/10.3390/foods13152309

Sun, J., Zhou, R., Qian, H., Li, Y., Zhang, H., Qi, X., & Wang, L. (2022). Investigation the influences of water-extractable and water-unextractable arabinoxylan on the quality of whole wheat you-tiao and its mechanism. Food Chemistry, 386, 132809. https://doi.org/10.1016/j.foodchem.2022.132809

Wan, J., Wei, Y., Zhang, Y., Lan, H., Li, X., Wang, Y., Luo, D., Feng, J., Bai, Z., & Guo, J. (2025). Innovative use of wastewater-extracted Arabinoxylans: Elevating steamed bread texture and structure. Food Chemistry, 466, 142120. https://doi.org/10.1016/j.foodchem.2024.142120

Wang, J., Cao, J., Xu, N., Meng, T., Zhang, G., & Zhang, Y. (2024). Ultrasound-enhanced covalent reaction of gliadin: The inhibition of antigenicity and its potential mechanisms. Journal of the Science of Food and Agriculture, 104(10), 6127–6138. https://doi.org/10.1002/jsfa.13436

Wang, N., Wu, L., Yang, J., You, Y., Zhang, F., Kan, J., & Zheng, J. (2023). Lotus starch/bamboo shoot polysaccharide composite system treated via ultrasound: Pasting, gelling properties and multiscale structure. Food Research International, 174, 113605. https://doi.org/10.1016/j.foodres.2023.113605

Wang, P., Wang, G., Zhang, Y., Lv, X., Xie, C., Shen, J., Yang, R., Gu, Z., Zhou, J., & Jiang, D. (2022). Impact of Wheat Arabinoxylan with Defined Substitution Patterns on the Heat-Induced Polymerization Behavior of Gluten. Journal of

Agricultural and Food Chemistry, 70(46), 14784–14797. https://doi.org/10.1021/acs.jafc.2c05236

Wang, P., Zhao, X., Yang, R., Zhou, Y., Zhou, Q., Gu, Z., & Jiang, D. (2020). Water-Extractable Arabinoxylan-Induced Changes in the Conformation and Polymerization Behavior of Gluten upon Thermal Treatment. Journal of Agricultural and Food Chemistry, 68(13), 4005–4016. https://doi.org/10.1021/acs.jafc.9b08122

Wang, P., Zou, M., Li, D., Zhou, Y., Jiang, D., Yang, R., & Gu, Z. (2020). Conformational rearrangement and polymerization behavior of frozen-stored gluten during thermal treatment. Food Hydrocolloids, 101, 105502. https://doi.org/10.1016/j.foodhyd.2019.105502

Wang, Q., Luo, D., Bai, Z., Yue, C., Li, P., & Han, S. (2026a). The effect of ultrasonic treatment on the properties of batter from medium-gluten flour and its mechanism of action. Innovative Food Science & Emerging Technologies, 110, 104492. https://doi.org/10.1016/j.ifset.2026.104492

Wang, Q., Luo, D., Bai, Z., Yue, C., Li, P., & Han, S. (2026b). The effect of ultrasonic treatment on the properties of batter from medium-gluten flour and its mechanism of action. Innovative Food Science & Emerging Technologies, 110, 104492. https://doi.org/10.1016/j.ifset.2026.104492

Wang, Q., Luo, D., Bai, Z., Yue, C., Li, P., & Han, S. (2026c). The effect of ultrasonic treatment on the properties of batter from medium-gluten flour and

its mechanism of action. Innovative Food Science & Emerging Technologies, 110, 104492. https://doi.org/10.1016/j.ifset.2026.104492

Wang, R.-X., Li, Y.-Q., Sun, G.-J., Wang, C.-Y., Liang, Y., Hua, D.-L., Chen, L., & Mo, H.-Z. (2023). The improvement and mechanism of gelation properties of mung bean protein treated by ultrasound. LWT, 182, 114811. https://doi.org/10.1016/j.lwt.2023.114811

Wang, T., Luo, D., Bai, Z., Yue, C., Li, P., & Han, S. (2026). Ultrasonic cavitation pretreatment of batter: A mechanism for optimizing dough properties. Food Chemistry, 498, 147114. https://doi.org/10.1016/j.foodchem.2025.147114

Wang, Y., Liu, J., Zhang, Z., Meng, X., Yang, T., Shi, W., He, R., & Ma, H. (2023a). Insights into Ultrasonication Treatment on the Characteristics of Cereal Proteins: Functionality, Conformational and Physicochemical Characteristics. Foods, 12(5), 971. https://doi.org/10.3390/foods12050971

Wang, Y., Liu, J., Zhang, Z., Meng, X., Yang, T., Shi, W., He, R., & Ma, H. (2023b). Insights into Ultrasonication Treatment on the Characteristics of Cereal Proteins: Functionality, Conformational and Physicochemical Characteristics. Foods, 12(5), 971. https://doi.org/10.3390/foods12050971

Yang, S., Zhang, Q., Yang, H., Shi, H., Dong, A., Wang, L., & Yu, S. (2022). Progress in infrared spectroscopy as an efficient tool for predicting protein secondary structure. International Journal of Biological Macromolecules, 206, 175–187. https://doi.org/10.1016/j.ijbiomac.2022.02.104

Yang, Y., Yang, L., Guan, E., & Bian, K. (2025). Investigation of the behavior of wheat flour dough under different sheeting-resting cycles and temperatures: Large deformation rheology and gluten molecular interactions. Food Chemistry: X, 27, 102366. https://doi.org/10.1016/j.fochx.2025.102366

Yu, X., Wang, X., Zou, L., Cai, K., Pan, J., & Chen, C. (2023). Insights into the in vitro digestibility of pork myofibrillar protein with different ionic polysaccharides from the perspective of gel characteristics. Food Chemistry, 426, 136520. https://doi.org/10.1016/j.foodchem.2023.136520

Yue, C., Tang, Y., Li, Z., Wang, X., Wang, L., Luo, D., Li, P., Han, S., Guo, J., & Bai, Z. (2025a). Ultrasound-assisted fermentation effectively alleviates the weakening of wheat gluten network caused by long-chain inulin and the underlying mechanism. Food Research International, 204, 115934. https://doi.org/10.1016/j.foodres.2025.115934

Yue, C., Tang, Y., Li, Z., Wang, X., Wang, L., Luo, D., Li, P., Han, S., Guo, J., & Bai, Z. (2025b). Ultrasound-assisted fermentation effectively alleviates the weakening of wheat gluten network caused by long-chain inulin and the underlying mechanism. Food Research International, 204, 115934. https://doi.org/10.1016/j.foodres.2025.115934

Zhang, J., Luo, D., Xiang, J., Xu, W., Xu, B., Li, P., & Huang, J. (2021a). Structural Variations of Wheat Proteins under ultrasound treatment. Journal of Cereal Science, 99, 103219. https://doi.org/10.1016/j.jcs.2021.103219

907 Zhang, J., Luo, D., Xiang, J., Xu, W., Xu, B., Li, P., & Huang, J. (2021b). Structural
908 Variations of Wheat Proteins under ultrasound treatment. Journal of Cereal
909 Science, 99, 103219. https://doi.org/10.1016/j.jcs.2021.103219
910 Zhang, J., Luo, D., Xiang, J., Xu, W., Xu, B., Li, P., & Huang, J. (2021c). Structural
911 Variations of Wheat Proteins under ultrasound treatment. Journal of Cereal
912 Science, 99, 103219. https://doi.org/10.1016/j.jcs.2021.103219
913 Zhang, J., Luo, D., Xiang, J., Xu, W., Xu, B., Li, P., & Huang, J. (2021d). Structural
914 Variations of Wheat Proteins under ultrasound treatment. Journal of Cereal
915 Science, 99, 103219. https://doi.org/10.1016/j.jcs.2021.103219
916 Zhang, M., Jia, R., Ma, M., Yang, T., Sun, Q., & Li, M. (2023). Versatile wheat
917 gluten: Functional properties and application in the food-related industry.
918 Critical Reviews in Food Science and Nutrition, 63(30), 10444–10460.
919 https://doi.org/10.1080/10408398.2022.2078785
920 Zhao, J., Ni, D., Bhandari, B., Gaiani, C., & Prakash, S. (2024). Impacts of oat flour
921 fortification on the rheological, microstructural, digestibility, and sensory
922 characteristics of low-fat, high-protein almond-based gels. Food
923 Hydrocolloids, 151, 109849. https://doi.org/10.1016/j.foodhyd.2024.109849
924 Zhao, J., Xie, W., Chen, Z., Zheng, Y., & Li, S. (2025). Enhancement of Dough
925 Processing and Steamed Bread Quality with Modified Soybean Residue
926 Dietary Fiber. Foods, 14(3), 346. https://doi.org/10.3390/foods14030346
927 Zhou, Y., Dhital, S., Zhao, C., Ye, F., Chen, J., & Zhao, G. (2021). Dietary
928 fiber-gluten protein interaction in wheat flour dough: Analysis, consequences

and proposed mechanisms. Food Hydrocolloids, 111, 106203. https://doi.org/10.1016/j.foodhyd.2020.106203

Zhu, Y., Li, F., Wang, Y., Li, J., Teng, C., Wang, C., & Li, X. (2019). Effects of different molecular weight water-extractable arabinoxylans on the physicochemical properties and structure of wheat gluten. Journal of Food Science and Technology, 56(1), 340–349. https://doi.org/10.1007/s13197-018-3494-2

Zhu, Y., Wang, Y., Li, J., Li, F., Teng, C., & Li, X. (2017a). Effects of Water-Extractable Arabinoxylan on the Physicochemical Properties and Structure of Wheat Gluten by Thermal Treatment. Journal of Agricultural and Food Chemistry, 65(23), 4728–4735. https://doi.org/10.1021/acs.jafc.7b00837

Zhu, Y., Wang, Y., Li, J., Li, F., Teng, C., & Li, X. (2017b). Effects of Water-Extractable Arabinoxylan on the Physicochemical Properties and Structure of Wheat Gluten by Thermal Treatment. Journal of Agricultural and Food Chemistry, 65(23), 4728–4735. https://doi.org/10.1021/acs.jafc.7b00837

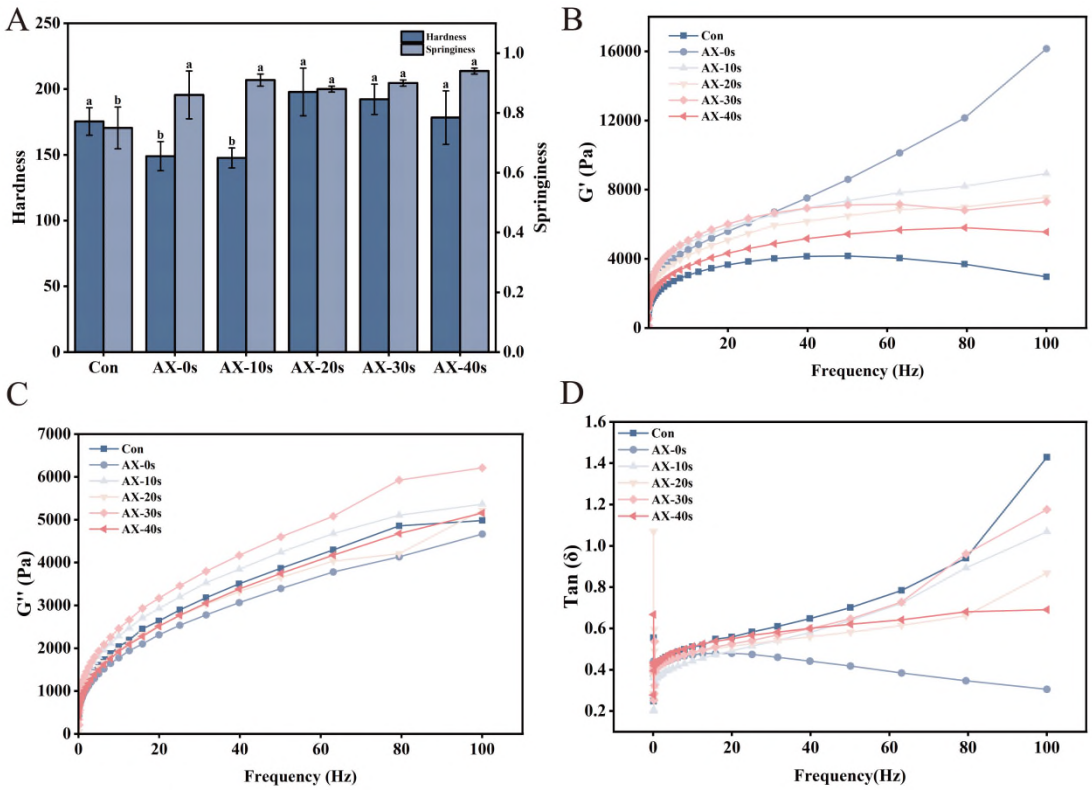


Fig. 1. **(A)** Texture data plot. **(B)**, **(C)**, and **(D)** show the G', G'', and Tan (δ) data plots, respectively.

Note: WEAX refers to water-extractable arabinoxylan. (10-40 s) refers to treatment groups with different ultrasound durations. Different lowercase letters indicate significant differences between groups ($p < 0.05$).

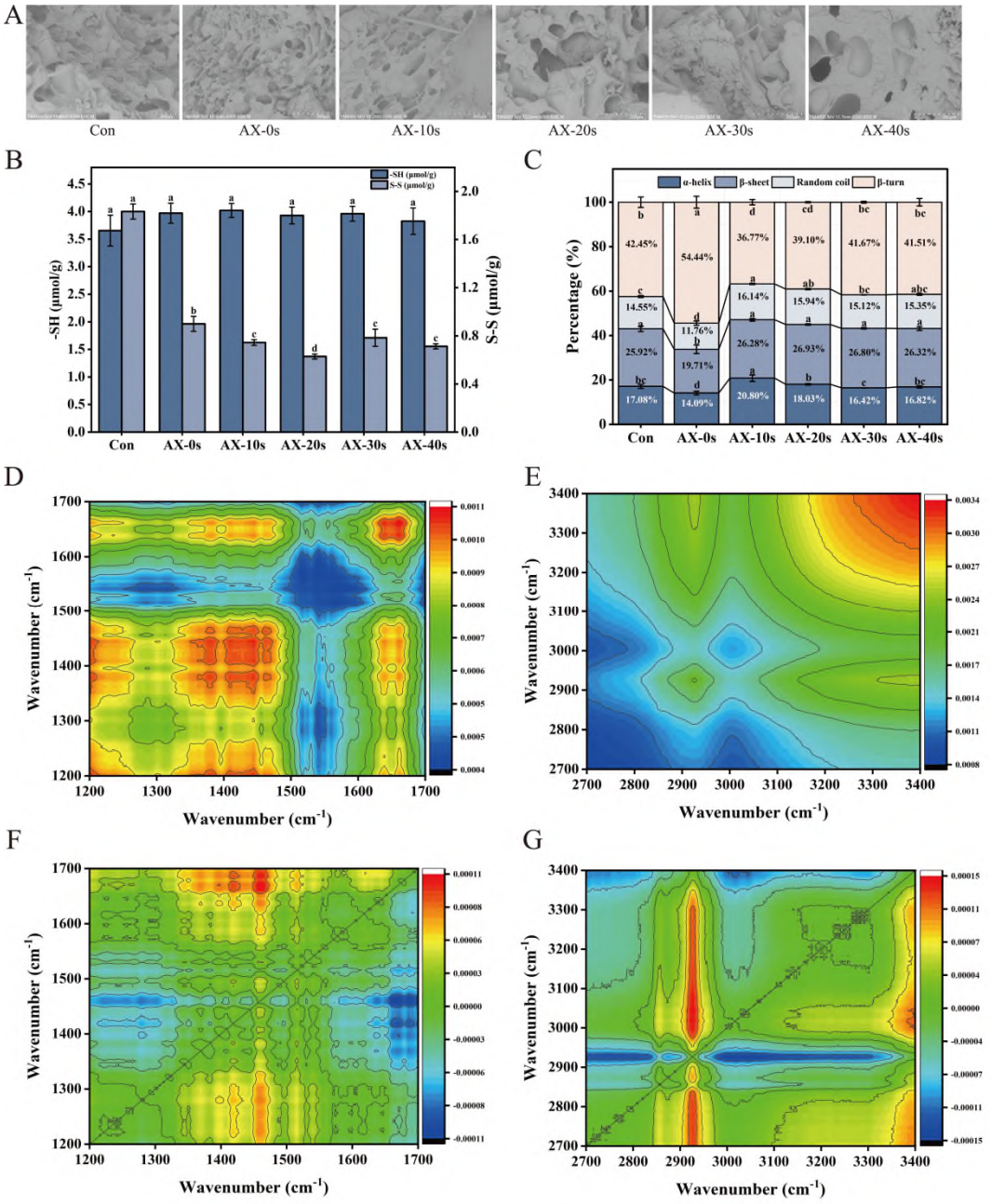


Fig. 2. **(A)** SEM micrograph. **(B)** -SH and S-S spectra. **(C)** Secondary structure diagram. **(D-F)** are 2D infrared correlation spectra (D and E: synchronous; F and G: asynchronous)

Note: WEAX refers to water-extractable arabinoxylan. (10-40 s) refers to treatment groups with different ultrasound durations. Different lowercase letters indicate significant differences between groups ($p < 0.05$).

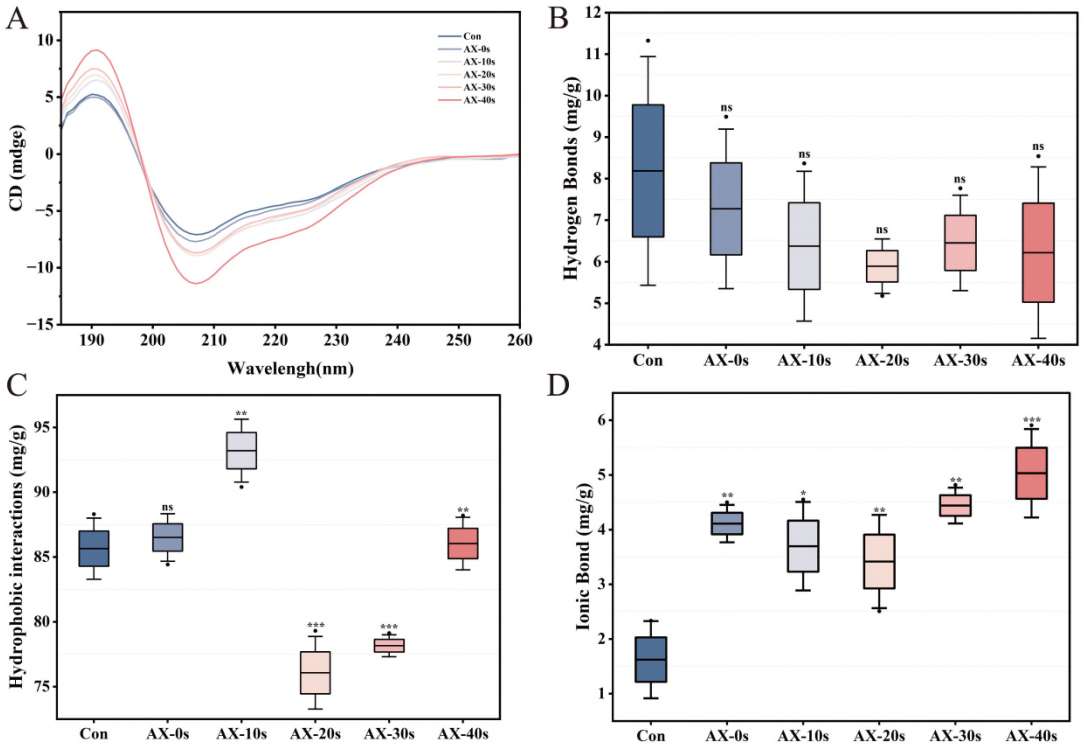


Fig. 3. **(A)** Circular dichroism data plot. **(B)**, **(C)**, and **(D)** show data plots for intermolecular interactions, representing hydrogen bonds, Hydrophobic interactions, and ionic bonds, respectively.

Note: WEAX refers to water-extractable arabinoxylan. (10-40 s) refers to treatment groups with different ultrasound durations. * indicates a comparison with Con, $p < 0.05$. ** indicates $p < 0.01$. *** indicates $p < 0.001$. ns indicates no significance. The horizontal line represents the median and the dots represent outliers.

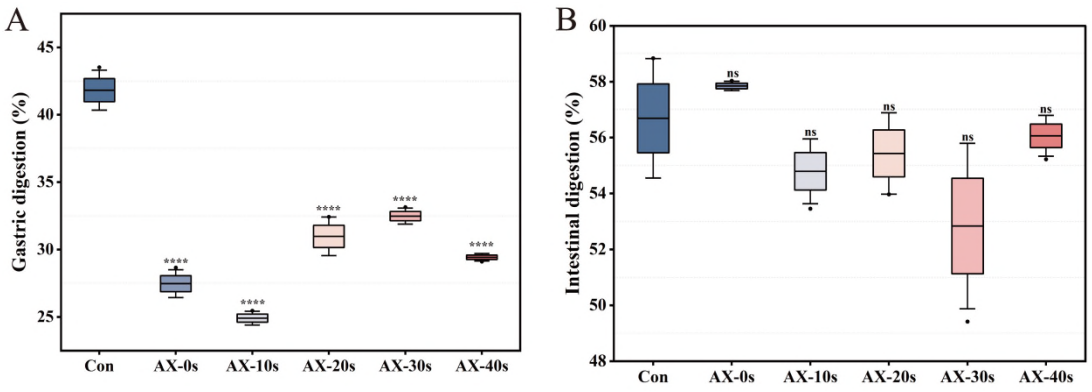


Fig. 4. (A) Graph of gastric digestion data. **(B)** Graph of intestinal digestion data.

Note: WEAX refers to water-extractable arabinoxylan. (10-40 s) refers to treatment groups with different ultrasound durations. * indicates a comparison with Con, $p < 0.05$. ** indicates $p < 0.01$. *** indicates $p < 0.001$. **** indicates $p < 0.0001$. ns indicates no significance. Horizontal lines represent medians and dots represent outliers.

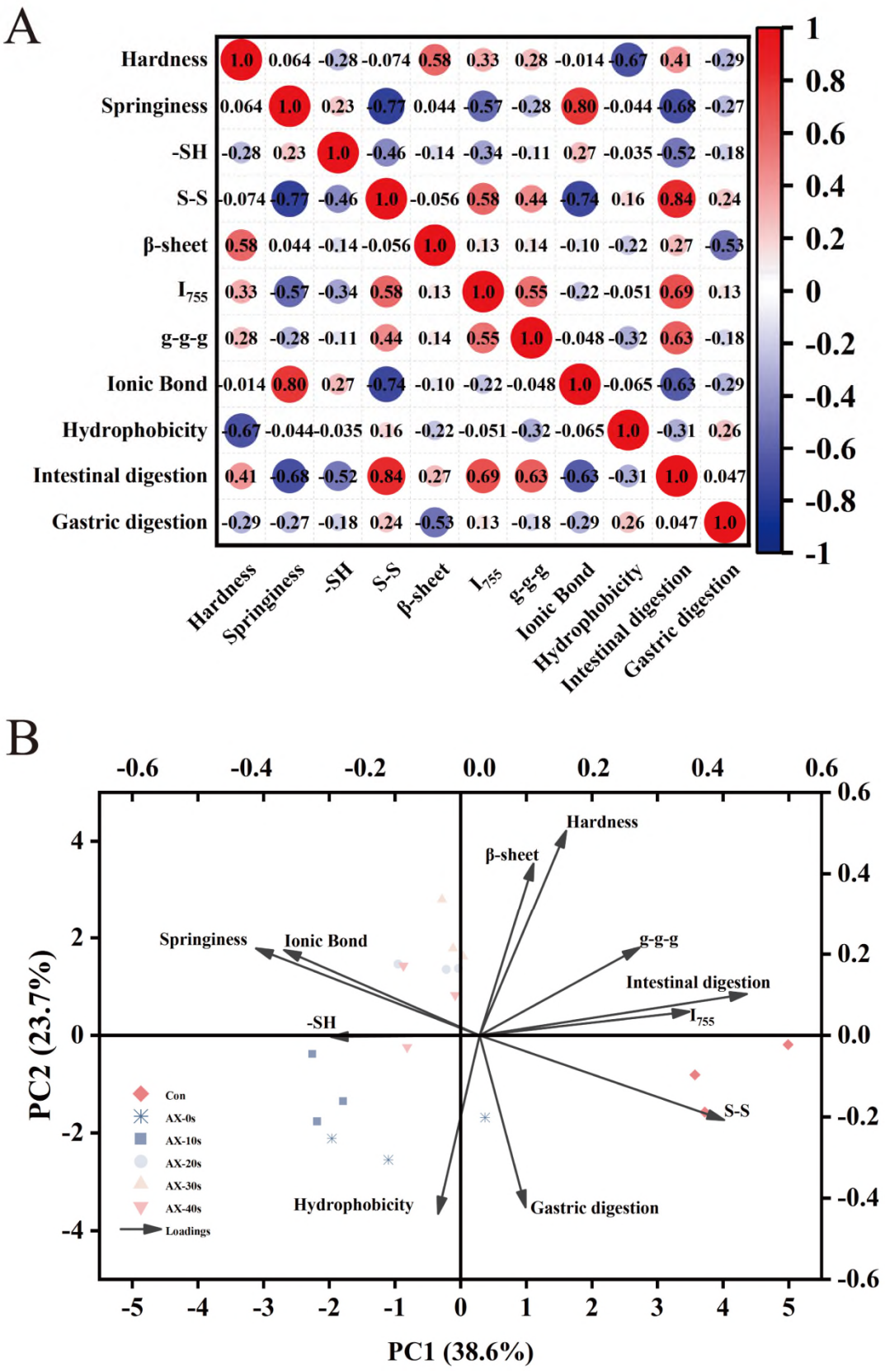


Fig. 5. **(A)** Correlation analysis plot of the glutenin-WEAX complex system with ultrasound. **(B)** Principal component analysis (PCA) data plot.

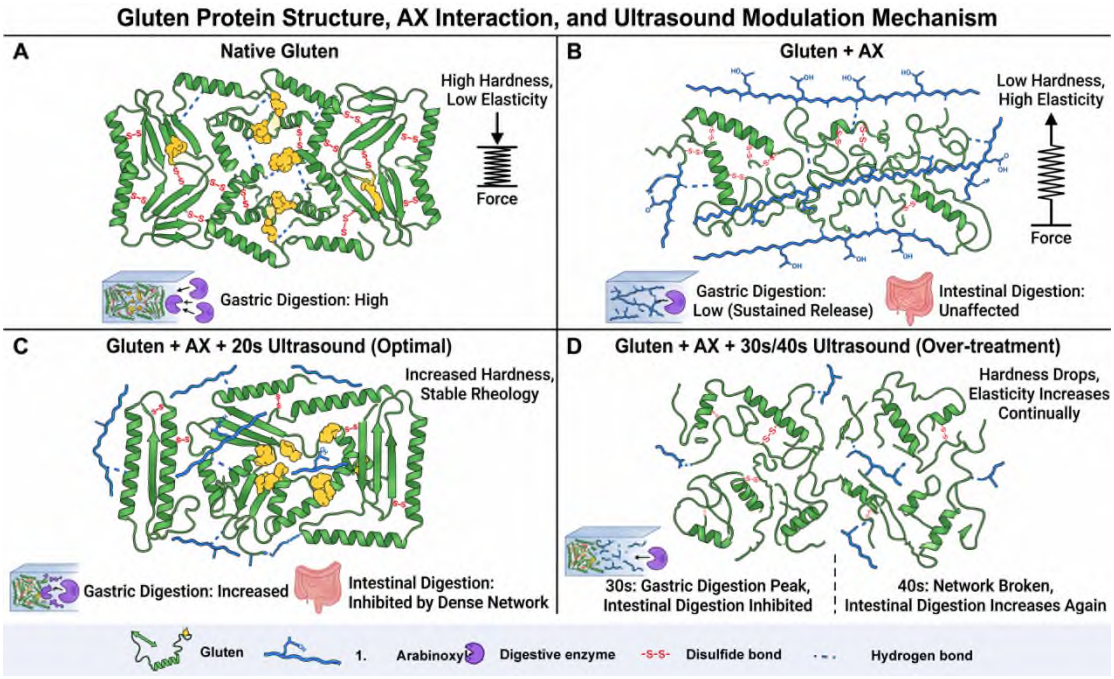


Fig. 6. Schematic Diagram Illustrating the Mechanism of Ultrasound-Assisted WEAX-Glutenin

Table 1. The data in the table show how the texture of the WEAX-gluten protein composite system changes when it is exposed to different ultrasonic treatments.

	Hardness	**Springiness**	**Cohesiveness**	**Resilience**	**Chewiness**
Con	175.35 ± 10.48^{a}	0.75 ± 0.07^{b}	0.86 ± 0.02^{abc}	0.30 ± 0.01^{b}	105.03 ± 2.09^{b}
AX-0 s	148.96 ± 11.05^{b}	0.86 ± 0.08^{a}	0.87 ± 0.01^{ab}	0.33 ± 0.04^{b}	108.25 ± 6.94^{b}
AX-10 s	147.64 ± 7.60^{b}	0.91 ± 0.02^{a}	0.84 ± 0.00^{bc}	0.31 ± 0.00^{b}	112.09 ± 6.93^{b}
AX-20 s	197.77 ± 18.08^{a}	0.88 ± 0.01^{a}	0.88 ± 0.03^{a}	0.31 ± 0.01^{b}	152.64 ± 8.37^{a}
AX-30 s	192.20 ± 11.58^{a}	0.90 ± 0.01^{a}	0.84 ± 0.02^{bc}	0.32 ± 0.00^{b}	144.68 ± 6.44^{a}
AX-40 s	178.30 ± 20.32^{a}	0.94 ± 0.01^{a}	0.83 ± 0.01^{c}	0.40 ± 0.02^{a}	142.41 ± 14.54^{a}

Note: WEAX refers to water-extractable arabinoxylan. (10-40 s) refers to treatment groups with different ultrasound durations. Different lowercase letters indicate significant differences between groups ($p < 0.05$).

Table 2. The data in the table are Raman spectra obtained after adding WEAX to gluten protein and subjecting it to various ultrasonic treatments.

	Aromatic amino acid environment		S-S bridges conformations (490-550cm^{-1})		
	I_{755}	**I_{850}/I_{830}**	**g-g-g (%)**	**t-g-g (%)**	**t-g-t (%)**
Con	1.194 ± 0.005^{a}	0.949 ± 0.005^{a}	17.70 ± 0.65^{b}	27.94 ± 0.25^{a}	54.36 ± 0.79^{a}
AX-0s	1.187 ± 0.006^{ab}	0.946 ± 0.002^{a}	16.65 ± 0.42^{ab}	27.95 ± 0.54^{a}	55.40 ± 0.95^{a}
AX-10s	1.183 ± 0.004^{a}	0.947 ± 0.001^{a}	15.78 ± 0.64^{a}	28.13 ± 0.95^{a}	56.09 ± 1.21^{a}
AX-20s	1.185 ± 0.002^{ab}	0.948 ± 0.002^{a}	16.55 ± 0.02^{ab}	27.84 ± 0.82^{a}	55.61 ± 0.81^{a}
AX-30s	1.189 ± 0.002^{ab}	0.949 ± 0.003^{a}	17.46 ± 1.14^{ab}	27.87 ± 0.42^{a}	54.67 ± 1.02^{a}
AX-40s	1.191 ± 0.001^{ab}	0.948 ± 0.003^{a}	17.38 ± 0.54^{ab}	28.42 ± 0.87^{a}	54.20 ± 0.11^{a}

Note: WEAX refers to water-extractable arabinoxylan. (10-40 s) refers to treatment groups with different ultrasound durations. Different lowercase letters indicate significant differences between groups ($p < 0.05$).

Supplementary Files

This is a list of supplementary files associated with this preprint. Click to download.

- Highlights.docx